JOURNAL OF PROPULSION AND POWER
Vol. 13, No. 6, November–December 1997

Effect of Wall Roughness on the Flow Through Converging–Diverging Nozzles

Venkata S. Krishnamurty* and Wei Shyy†
University of Florida, Gainesville, Florida 32611

An understanding of the effect of wall roughness on turbulent flows is important in many engineering applications. The roughness can affect both skin-friction and pressure drag through such factors as the thrust ratios, discharge coefficients, and static pressure distributions. The effect of roughness height on the performance of two-dimensional, converging–diverging nozzles is studied computationally. It is observed that while the total thrust decreases as the wall roughness increases, there is a tradeoff between the losses associated with the shock system and those associated with the skin-friction. However, the normalized skin-friction coefficient is seen to be virtually independent of the Mach number variation. An empirical correlation is proposed to fit the observed variation of skin-friction coefficient as a function of the roughness height.

Nomenclature

A	=	area of the control volume
A^+	=	damping function
a	=	speed of sound
C_d	=	mass flow coefficient
C_F	=	axial thrust coefficient
C_f	=	skin-friction coefficient
$C_{f,\mathrm{compr}}$	=	skin-friction coefficient for compressible flows
$C_{f,\mathrm{inc}}$	=	skin-friction coefficient for equivalent incompressible flows
C_p	=	specific heat at constant pressure
C_v	=	specific heat at constant volume
E	=	specific total energy
e	=	specific internal energy
H	=	specific total enthalpy
k	=	turbulent kinetic energy
k_r	=	wall roughness height
M	=	Mach number
Pr	=	Prandtl number
p	=	instantaneous static pressure
$\boldsymbol{q}_i$	=	heat flux vector
Re	=	Reynolds number
r	=	recovery factor
T	=	temperature
u_p	=	velocity component along the direction parallel to the wall
u_τ	=	friction velocity, $\sqrt{\tau_w/\rho_w}$
u^+	=	nondimensional velocity, u_p/u_τ
x, y	=	spatial coordinates
y^+	=	nondimensional distance, $\rho y u_\tau/\mu$, from the wall
γ	=	ratio of specific heats, C_p/C_v
δ_{ij}	=	Kronecker delta
ε	=	rate of dissipation of turbulent kinetic energy
κ	=	von Kármán constant, 0.41
μ	=	coefficient of viscosity
ν	=	coefficient of kinematic viscosity, μ/ρ
ρ	=	density
τ	=	viscous stress
$\bar{\ }$	=	Reynolds (ensemble) average
$\tilde{\ }$	=	Favre (mass-weighted average)

Subscripts

amb	=	ambient
compr	=	compressible flows
d	=	design condition
e	=	exit
eff	=	effective
inc	=	incompressible flows
L	=	laminar
p	=	parallel to the wall
t	=	turbulent or throat
w, wall	=	wall conditions
0	=	stagnation conditions
∞	=	freestream conditions
,	=	derivative in tensorial notation

Superscripts

$'$	=	fluctuations with respect to a Reynolds (ensemble) average
$''$	=	fluctuations with respect to a Favre (mass-weighted average)
$+$	=	nondimensional quantity

I. Introduction

THE performance of a nozzle is dependent on such factors as the geometry, the influence of friction, heat transfer, composition change, and shocks.[1] In this paper, we consider the influence of friction on the performance characteristics of two-dimensional converging–diverging nozzles. The accurate prediction of turbulent flows over rough surfaces is an important problem for many systems of engineering interest. Because the skin friction and other associated losses for the turbulent flow over a rough surface can be significantly larger than that for the corresponding flow over a smooth surface, and the nature of the flowfield over a rough and a smooth wall can be different, there is a practical need for accurate predictive capabilities to determine these losses to aid in the improvement of engineering designs. For many systems, rough walls cannot be avoided because of such factors as manufacturing limitations and wear. However, in many other situations, the presence of rough walls is the result of a tradeoff in which certain levels of additional friction losses are accepted to achieve other goals. An example is the use of acoustic tiles inside a supersonic jet engine nozzle.

Received March 23, 1997; revision received June 9, 1997; accepted for publication June 16, 1997.

*Graduate Student, Department of Aerospace Engineering, Mechanics, and Engineering Science; currently at Kohler Co., Fluid Mechanics Research, MC: 077, 444 Highland Drive, Kohler, WI 53044.

†Professor and Chairman, Department of Aerospace Engineering, Mechanics, and Engineering Science. Associate Fellow AIAA.

Various aspects of the effect of surface roughness on the skin-friction drag problem have been treated by many investigators in the low-speed incompressible flow case. The most systematic experimental investigation of both the skin-friction drag and the development of the boundary-layer structure on a rough surface was carried out by Nikuradse (see Ref. 2, p. 654).

The conventional engineering representation of the wall friction gives the wall shear stress τ_{wall} as

$$\tau_{\mathrm{wall}} = c_f(\rho u_\infty^2/2) \tag{1}$$

Based on dimensional arguments,[3] the skin-friction coefficient depends upon the Mach and Reynolds numbers and the roughness of the wall, i.e.,

$$c_f = c_f(M, Re, k_r) \tag{2}$$

where k_r is a dimensionless measure of the surface roughness. On a smooth wall, an increase in Mach number results in a decrease in the skin-friction coefficient, thereby thickening the laminar sublayer. When the wall is rough, the influence of Mach number on skin friction is even greater. According to Liepmann and Goddard[4] and Goddard,[5] the ratio $c_{f,\mathrm{compr}}/c_{f,\mathrm{inc}}$ for the completely rough regime becomes proportional to the density ratio $\rho_{\mathrm{wall}}/\rho_\infty$. A simple rule for the effect of Mach number on the drag of a fully rough surface is given as (for flat-plate boundary layers)[4]

$$\frac{c_{f,\mathrm{compr}}}{c_{f,\mathrm{inc}}} = \frac{1}{1 + r[(\gamma - 1)/2]M_\infty^2} \tag{3}$$

However, from his experimental measurements, Goddard[5] observes that the Mach number has little effect on the ratio c_f/c_{f0}, where c_f is the coefficient for rough walls, and c_{f0} is the coefficient for smooth walls. Goddard[5] remarks that the "effect of surface roughness on skin-friction drag is localized deep within the boundary layer at the surface itself and is independent of the external flow, i.e., Mach number, per se, is eliminated as a variable." Computational studies conducted by Wilcox[6] support the viewpoint that Mach number has little effect on predicted values of c_f/c_{f0}. The observations in the preceding text of the effect of surface roughness on the skin-friction coefficient are for flat-plate boundary layers, and there is little information on the effect of wall roughness on compressible flow with pressure gradients. This study is, in part, motivated to extend our knowledge of flat-plate flows to two-dimensional converging–diverging nozzle flowfields. The other motivation is to gain insight into the relative role of skin-friction and shock-induced pressure loss in turbulent shear flows in the presence of wall roughness.

In Sec. II, a brief review of the literature is presented with a discussion of relevant experimental and numerical modeling approaches to study the effect of wall roughness. A description of the modifications used in this computational work (in the framework of the k-ε model) is also presented. Details of the computational study are presented in Sec. III. Section IV presents a discussion of the results obtained in this computational study. Section V concludes this paper with remarks on the outcome of this computational study.

II. Physical Models of Wall Roughness

A. Literature Review

Approaches to modeling wall roughness broadly include 1) momentum integral methods, 2) equivalent sand-grain roughness approaches, and 3) discrete-element approaches. Momentum integral methods rely on empirical correlation for skin-friction coefficient and boundary-layer entrainment to predict the evolution of turbulent boundary layers over rough walls. These methods are of limited applicability primarily because of restrictive assumptions about the flow at the wall, and they are not considered here. The latter two approaches can be directly employed within the framework of computational procedures based on the Navier–Stokes equations and are of primary concern.

The equivalent sand-grain approach to roughness is sufficient for surfaces with distributed roughness for which an effective sand-grain height can be found. Some questions can be raised regarding the usefulness of this approach for surfaces with localized roughness features. One fundamental issue of concern is the validity of the assumption that the boundary conditions based on the law of the wall hold (which is modified by simply shifting the origin of the reference point according to the roughness length scale), for surfaces with large enough discrete local roughness features. Such features may completely change the local flow structure in the vicinity of the wall because of the local generation of vorticity. Another more practical issue of concern is that of determining the equivalent sand-grain roughness height, which is an inherently distributed property, for a surface with discrete local roughness profiles.

To obviate the use of an equivalent sand-grain roughness and to gain a greater understanding of the influence of local roughness effects on turbulent skin-friction production, the discrete-element approach has been employed by several researchers. In this approach, the rough surface elements are treated as individual protrusions into the flow past an otherwise smooth wall. The primary contributions to the overall losses at the wall are assumed to come from both local skin-friction and form drag as a result of the protrusion of the roughness elements from the wall. The contribution of form drag to the overall resistance at the wall is one significant element that is unaccounted for in the equivalent sand-grain approach. Many implementations of the basic discrete-element approach have been developed.[7–11] Common to most of these methods is the introduction of blockage factors into the transport equations to account for the reduced cross-sectional area provided to the flow because of the presence of the roughness elements. In addition, most of these methods incorporate an explicit form drag term in the momentum equations. Use of the discrete-element approach has mostly concentrated on the prediction of turbulent flow over an evenly spaced array of objects, although some progress in the area of stochastic roughness has been made.[11] Most of these models have been correlated with experimental data for relatively simplified flows with discrete elements of fixed shape, including cones, spheres, and squares.

In the present work, the sand-grain roughness modeling approach is adopted. One reason is that for many applications, an effective sand-grain roughness height for a rough surface can be successfully and practically determined. Moreover, the equivalent sand-grain roughness concept can be conveniently and effectively incorporated in two-equation models of turbulence that are still the model of choice for most practical engineering applications. However, since shock strength and location vary with the sand-grain thickness, the overall effect of wall roughness must account for the form drag as well. In the following, we will discuss the approach that has been taken to incorporate the sand-grain roughness concept in two-equation models.

B. Modifications

The equivalent sand-grain roughness concept was initiated to utilize the rough wall skin-friction data compiled by Nikuradse (Ref. 2, p. 654). The equivalent sand-grain roughness for a given surface is defined as the sand-grain size in Nikuradse's experiments that produces the same skin-friction loss at the surface. The application of the equivalent sand-grain roughness approach is most often used in the framework of two-equation turbulence models. The effect of wall roughness on the law of the wall is usually incorporated by an upward shifting of the effective origin of the coordinate normal to the rough surface. Such a shift in the plane of reference from the wall location to a lower position is used to reflect the lower rate of turbulent momentum exchange for a rough wall vs a smooth wall under identical freestream conditions.

As far as the effect of equivalent sand-grain roughness is concerned, the approach normally taken is to incorporate the length of the sand-grain roughness into the turbulence model, to modify the predicted velocity profile. Several alternatives have been employed. For example, in the turbulence models employing the Van Driest formula for the mixing length, the following modification is made to account for roughness[12]:

$$l^+ = \kappa(y^+ + \Delta y^+)\left[1 - \exp\left(-\frac{y^+ + \Delta y^+}{A^+}\right)\right] \tag{4}$$

where l^+ is the nondimensional length-scale, and $y^+ = yu_\tau/\nu$ is the nondimensional distance from the wall (wall coordinate). The shift in the wall coordinate Δy^+ is a function of the sand-grain roughness parameter $k_r^+ = k_r u_\tau/\nu$:

$$\Delta y^+ = 0.9\,\{\sqrt{k_r^+} - k_r^+ \exp[-(k_r^+/6)]\} \tag{5}$$

A^+ in Eq. (4) is a damping function. Cebeci and Chang[7] define it as a function of the pressure gradient while using Eq. (5). Krogstad[13] has also employed a version of this model with some modifications.

In the present work, we have used the high-Reynolds number version of the k-ε model with the wall functions (modified to account for surface roughness), which is the turbulence model commonly adopted in many engineering calculations. For compressible flows, certain modifications to the k-ε model are necessary and have been proposed.[14] However, in the present Mach number range, the impact of these modifications is negligible.

The two-equation models of eddy–viscosity offer a viable approach to obtain information regarding the average variations in the flowfield. To solve the compressible turbulent flowfield, we made use of a mixed-averaging technique, whereby the velocity components and the temperature are averaged using a mass-weighted averaging procedure and the density and pressure are Reynolds averaged. Accordingly, the variables are split into their mean and average as follows:

$$\begin{aligned} \rho &= \bar{\rho} + \rho' \\ u_i &= \tilde{u}_i + u_i'' \\ p &= \bar{p} + p' \\ T &= \tilde{T} + T'' \end{aligned} \tag{6}$$

In the following equations (in their averaged form) we will drop the overbar and the tilde.

The equations of motion in their averaged, modeled form are given as

$$\frac{\mathrm{D}}{\mathrm{D}t}(\rho) + \rho\frac{\partial u_j}{\partial x_j} = 0 \tag{7}$$

$$\frac{\mathrm{D}}{\mathrm{D}t}(\rho u_j) = -\frac{\partial p}{\partial x_j} + \frac{\partial}{\partial x_i}\left(\sum_{ji}\right) \tag{8}$$

$$\frac{\partial}{\partial t}(\rho E) + \frac{\partial}{\partial x_j}(\rho u_j H) = \frac{\partial}{\partial x_i}\left(u_j\sum_{ji} - q_i + \Gamma_k\frac{\partial k}{\partial x_i}\right) \tag{9}$$

where

$$\frac{\mathrm{D}}{\mathrm{D}t} = \frac{\partial}{\partial t} + u_j\frac{\partial}{\partial x_j} \tag{10}$$

Table 1 Nozzle design parameters[18]

Parameter	A_e/A_t	l, cm	M_d	NPR_d	r_c, cm	θ, deg	α, deg
Nozzle A1	1.09	11.56	1.35	2.97	0.68	20.84	1.21
Nozzle B1	1.80	11.56	2.08	8.81	0.68	20.84	10.85

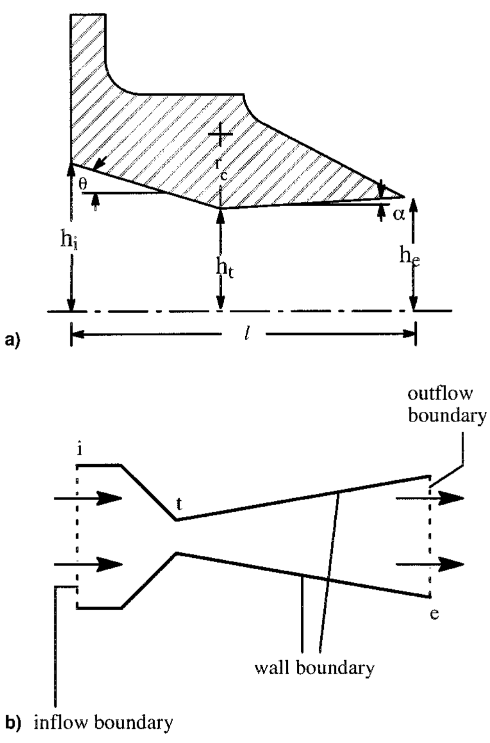

Fig. 1 Nozzle geometry and computational domain[18]: a) geometry and b) computational domain with relevant boundaries.

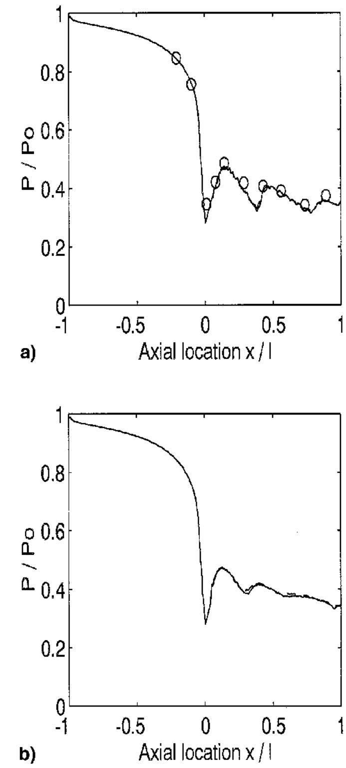

Fig. 2 Grid independence test; comparison of pressure distribution along the nozzle upper wall. ——, 297 × 61 grid; - - -, 297 × 101 grid, and 0, experiment.[18] Nozzle A1: a) smooth wall and b) rough wall, $k_r = 10^{-3}$.

Table 2 Comparison of nozzle performance parameters (nozzle A1) for the two grid systems

	Smooth wall			Rough wall: $k_r = 10^{-3}$		
Case	297 × 61	297 × 101	Change	297 × 61	297 × 101	Change
C_d	0.9598	0.9603	0.0005	0.9590	0.9599	0.0009
C_F	0.9672	0.9691	0.0019	0.9591	0.9622	0.0031

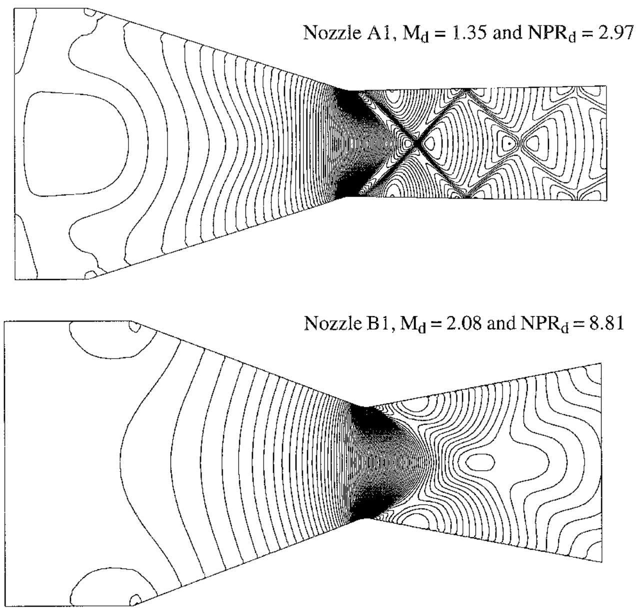

Fig. 3 Contour plot of computed static pressure variation in nozzles A1 and B1. The main difference between the two cases is the shock structure.

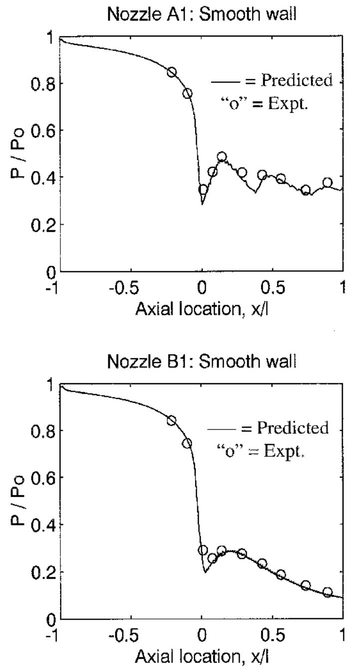

Fig. 4 Comparison of predicted values of static pressure (along the nozzle wall) with experimental measurements.[18]

In Eq. (9), E and H are written as

$$E = e + \tfrac{1}{2}u_iu_i + \tfrac{1}{2}\overline{u_i''u_i''} \tag{11}$$

$$\rho H = \rho E + p \tag{12}$$

$$\sum_{ij} = 2\mu_{\text{eff}}S_{ij} - \frac{2}{3}\mu_{\text{eff}}\frac{\partial u_k}{\partial x_k}\delta_{ij} \tag{13}$$

where $S_{ij} = \frac{1}{2}[(\partial u_i/\partial x_j) + (\partial u_j/\partial x_i)]$. $q_i = -k_{\text{eff}}(\partial T/\partial x_i)$ is the heat flux vector. μ_{eff} and k_{eff} are given as

$$\mu_{\text{eff}} = \mu_L + \mu_t \tag{14}$$

$$k_{\text{eff}} = \frac{\gamma}{\gamma - 1}\left(\frac{\mu_L}{Pr_L} + \frac{\mu_t}{Pr_t}\right) \tag{15}$$

In all of the computational results presented in this paper, the value of γ is set equal to 1.4, and the values of Pr_L and Pr_t are set equal to, respectively, 0.72 and 0.9. μ_t is obtained from a solution of the transport equations for turbulent kinetic energy k and its dissipation rate ε.

The equations of the standard high-Reynolds number version of the k-ε model are

$$\mu_t = C_\mu\rho(k^2/\varepsilon) \tag{16}$$

$$\frac{D}{Dt}(\rho k) = P_k - \rho\varepsilon + \frac{\partial}{\partial x_j}\left(\Gamma_k\frac{\partial k}{\partial x_j}\right) \tag{17}$$

$$\frac{D}{Dt}(\rho\varepsilon) = C_{\varepsilon 1}\frac{\varepsilon}{k}P_k - C_{\varepsilon 2}\rho\frac{\varepsilon^2}{k} + \frac{\partial}{\partial x_j}\left(\Gamma_\varepsilon\frac{\partial \varepsilon}{\partial x_j}\right) \tag{18}$$

where

$$P_k = -\overline{\rho u_i''u_j''}\frac{\partial u_i}{\partial x_j} \tag{19}$$

$$\Gamma_k = [\mu_L + (\mu_t/\sigma_k)] \quad \text{and} \quad \Gamma_\varepsilon = [\mu_L + (\mu_t/\sigma_\varepsilon)] \tag{20}$$

The constants in Eqs. (16–20) are prescribed to be

$$C_\mu = 0.09, \quad C_{\varepsilon 1} = 1.43, \quad C_{\varepsilon 2} = 1.92, \quad \sigma_k = 1.0, \quad \sigma_\varepsilon = 1.3 \tag{21}$$

A simple way of accounting for roughness, using the k-ε model, is via a modification of the boundary conditions. The most common approach uses the wall functions for the velocity, temperature, and turbulent kinetic energy, and its dissipation rate, which are specified at the first grid location from the solid boundary. The specification of boundary conditions at the first grid location makes oversimplifying assumptions about the location of the numerical grid point within the turbulent boundary layer. The grid point is usually chosen to lie in the logarithmic region (of the boundary layer on a wall). The wall functions used to prescribe the distribution of velocity and temperature are modified by incorporating k_r^+ in the expressions, to account for roughness.

For the wall function treatment, the velocity is assumed to obey a universal profile of the following form, for smooth walls:

$$u^+ = (u_p/u_\tau) = (1/\kappa)\ell n(y^+) + B \tag{22}$$

where $y^+ = yu_\tau/\nu$, $u_\tau = \sqrt{\tau_{\text{wall}}/\rho}$ represents the friction velocity,

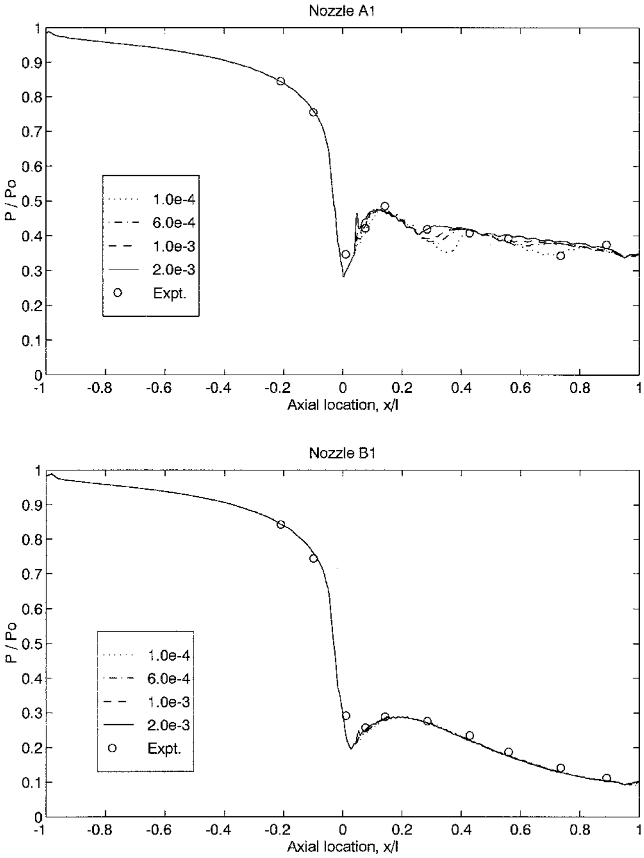

Fig. 5 Comparison of predicted values of static pressure (along the nozzle upper wall) with various k_r, with experimental data for smooth walls.

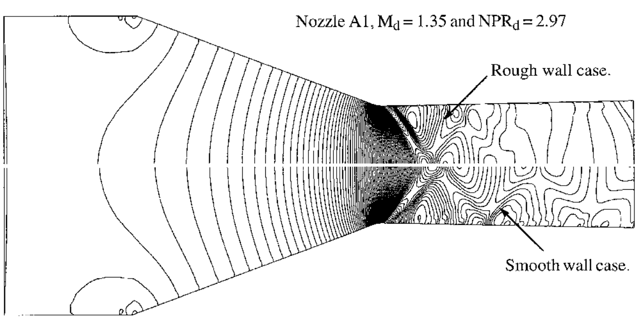

Fig. 6 Comparison of computed values of pressure (for nozzle A1) between the smooth and the rough walls with nondimensional k_r 1.0$e-3$.

u_p is the velocity magnitude parallel to the wall, and $B = 5.1$. Following some manipulations, the value of the wall shear stress can be expressed as

$$\tau_{\text{wall}} = \frac{\rho C_\mu^{1/4} k^{1/2} u_p}{u^+} \tag{23}$$

More details can be found in Shyy et al.[15]

The upward shift of the effective origin of the normal wall coordinate can be translated into an equivalent shift in the logarithmic profile (of the velocity in the inner layer), resulting in a modified form of the standard universal law-of-the-wall correlation:

$$u^+ = (1/\kappa)\ell n(y^+) + 5.5 - \Delta B(k_r^+) \tag{24}$$

The term $\Delta B(k_r^+)$ represents the downward shift in the velocity

Table 3 Mass flow and axial thrust coefficients

Case	Predicted value	Smooth-wall experimental and predicted data
	a) Nozzle A1[a]	
Smooth:	$C_d = 0.9598$	$\Delta C_d = 0.0202$
Turbulent	$C_F = 0.9672$	$\Delta C_F = 0.0228$
Rough:	$C_d = 0.9599$	$\Delta C_d = 0.0201$
$k_r = 0.0001$	$C_F = 0.9640$	$\Delta C_F = 0.026$
Rough:	$C_d = 0.9599$	$\Delta C_d = 0.0201$
$k_r = 0.0002$	$C_F = 0.9627$	$\Delta C_F = 0.0273$
Rough:	$C_d = 0.9598$	$\Delta C_d = 0.0202$
$k_r = 0.0004$	$C_F = 0.9618$	$\Delta C_F = 0.0282$
Rough:	$C_d = 0.9596$	$\Delta C_d = 0.0204$
$k_r = 0.0006$	$C_F = 0.9609$	$\Delta C_F = 0.0291$
Rough:	$C_d = 0.9591$	$\Delta C_d = 0.0209$
$k_r = 0.0008$	$C_F = 0.9595$	$\Delta C_F = 0.0305$
Rough:	$C_d = 0.9590$	$\Delta C_d = 0.021$
$k_r = 0.001$	$C_F = 0.9591$	$\Delta C_F = 0.0309$
Rough:	$C_d = 0.9590$	$\Delta C_d = 0.021$
$k_r = 0.002$	$C_F = 0.9578$	$\Delta C_F = 0.0322$
	b) Nozzle B1[b]	
Smooth:	$C_d = 0.9612$	$\Delta C_d = 0.0188$
Turbulent	$C_F = 0.9668$	$\Delta C_F = 0.0157$
Rough:	$C_d = 0.9613$	$\Delta C_d = 0.0187$
$k_r = 0.0001$	$C_F = 0.9653$	$\Delta C_F = 0.0172$
Rough:	$C_d = 0.9613$	$\Delta C_d = 0.0187$
$k_r = 0.0002$	$C_F = 0.9647$	$\Delta C_F = 0.0178$
Rough:	$C_d = 0.9614$	$\Delta C_d = 0.0186$
$k_r = 0.0004$	$C_F = 0.9643$	$\Delta C_F = 0.0182$
Rough:	$C_d = 0.9614$	$\Delta C_d = 0.0186$
$k_r = 0.0006$	$C_F = 0.9639$	$\Delta C_F = 0.0186$
Rough:	$C_d = 0.9613$	$\Delta C_d = 0.0187$
$k_r = 0.0008$	$C_F = 0.9635$	$\Delta C_F = 0.019$
Rough:	$C_d = 0.9614$	$\Delta C_d = 0.0186$
$k_r = 0.001$	$C_F = 0.9634$	$\Delta C_F = 0.0191$
Rough:	$C_d = 0.9613$	$\Delta C_d = 0.0187$
$k_r = 0.002$	$C_F = 0.9625$	$\Delta C_F = 0.02$

[a]Area ratio, 1.09 and NPR_d, 2.97. Experimental values: C_d, 0.98 and C_F, 0.99.
[b]Area ratio, 1.80 and NPR_d, 8.81. Experimental values: C_d, 0.98 and C_F, 0.9825.

profile and is dependent on the nondimensional roughness parameter $k_r^+ = k_r u_\tau / \nu$. It has been found that $\Delta B(k_r^+)$ is not a unique function of k_r^+, but depends on the type of roughness. A functional form for $\Delta B(k_r^+)$ has been proposed as follows, which spans the whole range of k_r^+, from hydraulically smooth ($k_r^+ \leq 5$), to transitionally smooth ($5 \leq k_r^+ \leq 60$), to fully rough ($k_r^+ \geq 60$):

$$\Delta B(k_r^+) \simeq (1/\kappa)\ell n(1 + 0.3k_r^+) \tag{25}$$

The correlation given by Eq. (25) matches the experimental data assembled by Clauser (see Ref. 16, p. 426). Other correlations have been proposed, as reviewed by Koh.[17] Basically, these formulas all share the same concept proposed by Rotta,[12] who assumed that the universal law of the wall applied to both smooth and rough walls.

III. Computational Technique and Flow Configuration

An application where the prediction of wall roughness effect is of interest is in the high-speed flow through nozzles. Any roughness at the nozzle walls could lead to a deterioration in the nozzle performance in terms of a loss in total pressure, axial thrust, etc. Hence, a reliable prediction of the effect of surface roughness will be a valuable contribution to the design and manufacture of nozzles.

Experimental measurements on the turbulent flow through two-dimensional converging–diverging nozzles (with smooth

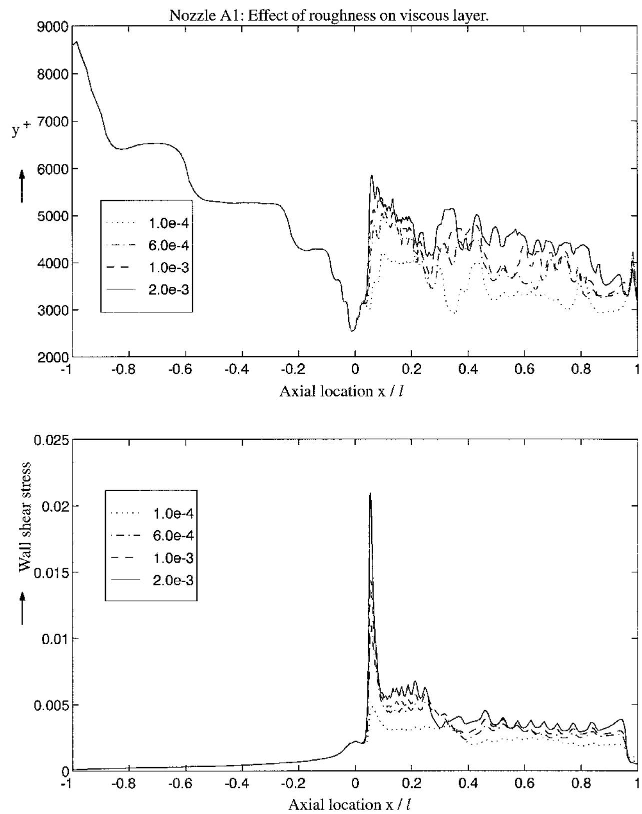

Fig. 7 Variation of y^+ and wall shear stress with various k_r for nozzle A1.

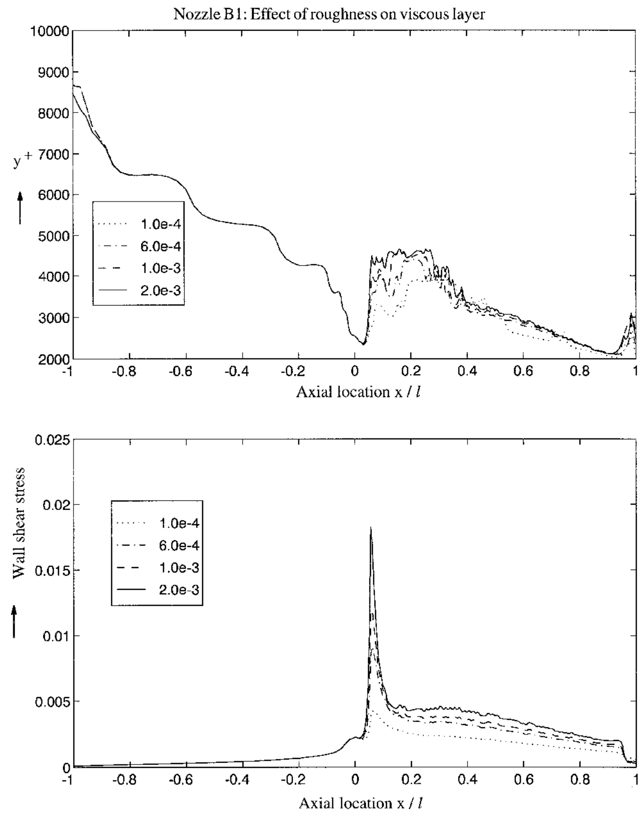

Fig. 8 Variation of y^+ and wall shear stress with various k_r for nozzle B1.

walls) have been conducted by Mason et al.[18] These experimental measurements are used to validate our computational studies of the turbulent flow over a smooth wall (for a converging–diverging nozzle). A sketch of the nozzle geometry and the boundaries (of the computational domain) are presented in Figs. 1a and 1b. The inlet plane, the throat, and the exit plane are denoted as i, t, and e, respectively. Table 1 gives details of the nozzle geometry and other relevant parameters. The notation used is identical to those in the report of Mason et al.[18] M_d denotes the design Mach number, NPR_d is the design nozzle pressure ratio, and r_c denotes the circular arc throat radius.

To conduct computational analysis of the nozzle flowfield, a numerical domain similar to that shown in Fig. 1b was used. The computations were conducted using the computational capability developed by Krishnamurty,[14] which employs the finite volume, multistage Runge–Kutta time-stepping scheme developed by Jameson et al.[19]

The computational domain is comprised of an inflow boundary, wall boundary, and an outflow boundary, as shown in Fig. 1b. At the inflow boundary, the stagnation pressure and stagnation enthalpy were held constant and the inflow Mach number is specified to be 0.23. The Reynolds number based on the inlet height is 5.807×10^6. At the exit boundary, conditions are obtained by extrapolation from the interior of the domain because the flow in the diverging portion of the nozzle is supersonic. At the wall boundaries, the wall functions have been used to prescribe the wall shear stress and boundary conditions for the turbulent kinetic energy and its dissipation rate. The walls are assumed to be adiabatic.

IV. Results and Discussion

A. Grid Independency

Computations were performed on two different grids (for nozzle A1) to evaluate the dependence of the solution obtained on the grid system used. Two grids, 1) with 297×61 and 2) with 297×101 grid points, were used in this test. Care was taken to ensure that the first grid point was at a location of $\Delta y^+ = 20$–40, as required by the wall-function treatment for the k-ε model. Figure 2 shows the comparison between the solutions obtained using the two grid systems. Figure 2a presents the comparison between the grid systems for the smooth wall (turbulent) case, and Fig. 2b presents the comparison for the rough wall case with roughness height $k_r = 10^{-3}$. The pressure distributions are essentially identical for the two grid systems. The nozzle performance parameters also indicated very little difference between the two grid systems. The mass flux and axial thrust coefficients, defined in the Appendix, are presented in Table 2 (for the two grid systems). It is evident that there is minimal change in the values obtained; in fact, the difference between the values obtained using the two grid systems is less than 0.5%. Therefore, all of the solutions presented through the remainder of this paper have been obtained using the 297×61 grid system for nozzle A1 and the 277×61 grid system for nozzle B1.

B. Comparison with Experiment: Smooth Wall

Figure 3 shows representative contour plots of the static pressure variation in the two nozzles listed in Table 1. The plots are presented to give a general idea of the structure of the flowfield and to aid in the subsequent discussion. Comparisons have been made of the predicted pressure distribution along the nozzle wall (with the experimental values) (Fig. 4). Computations were performed with both the artificial-dissipation scheme developed by Jameson et al.[19] and a second-order flux-vector splitting, Steger-Warming (upwind) scheme.[20] The artificial-dissipation scheme seemed to diffuse the discontinuities to a greater extent (compared to the upwind scheme). All of the results presented have been obtained using the second-order, flux-vector splitting scheme. Computations were also performed with the modifications to the k-ε model proposed by Sarkar et al.,[21] for the extra dissipation caused by compressibility. No noticeable difference exists in the result ob-

Table 4 Computed values of C_{f0}

Case	Smooth wall	Roughness k_r 1.0e−4	2.0e−4	4.0e−4	6.0e−4	8.0e−4	1.0e−3	2.0e−3
Nozzle A1	0.0194	0.0248	0.0264	0.0277	0.0289	0.0295	0.0299	0.0321
Nozzle B1	0.0275	0.0313	0.0324	0.0334	0.0342	0.0349	0.0352	0.0367

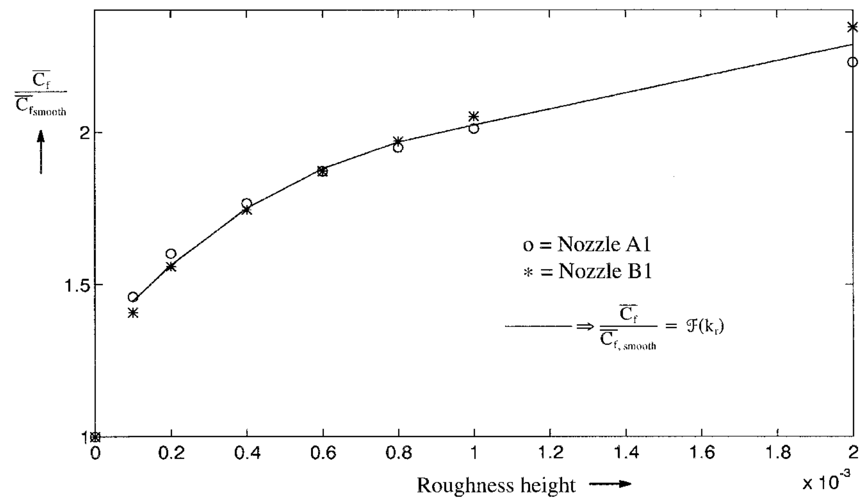

Fig. 9 Computed variation of normalized, average skin-friction coefficient with roughness height.

tained in comparison with the unmodified model. All of the computational results to be presented in this section have therefore been performed without any explicit modification accounting for compressibility.

C. Rough Wall Computations

Rough wall computations were performed with the modified wall-function treatment (to account for sand-grain roughness) described in Sec. II. The wall was assumed to be rough in the region x/l = 0.05–0.95 (the throat of the nozzle is at x/l = 0). For the modified wall-function computations, the roughness was assumed to comprise uniformly distributed roughness elements of nondimensional heights ranging from 10^{-4} to 2.0×10^{-3}. The nondimensionalization is with respect to the inlet height of the nozzle.

There is no known experimental information on the flow through nozzles with wall roughness in the unclassified literature. However, the information presented next is consistent with our experiences in cases where experimental guidance is available. Figure 5 presents a comparison of the pressure distribution (for the various roughness heights) along the nozzle upper wall with the experimental data for smooth walls. In the case of nozzle A1, the increase in roughness height is seen to result in a shift in the location of the peaks (in the pressure distribution) and an overall smearing of the shock system, which is especially evident in the profiles at the higher roughness heights. Nozzle B1, on the other hand, shows negligible differences in terms of the pressure distribution (along the nozzle wall) for the various roughness heights. The reason for the increased impact of roughness height observed in the flow through nozzle A1 is because of the multiple shock reflections resulting in a stronger interaction with viscous effects. The comparison of pressure contours presented in Fig. 6 clearly shows the shift in the location of the shocks (peaks in the pressure profiles) and the smearing of the peaks in the pressure profile (shown in Fig. 6).

To evaluate the effect of wall roughness on the performance of the nozzle, the mass flow and axial thrust coefficients are computed using the equations given in the Appendix. The values for both the nozzle geometries (A1 and B1) are given in Table 3 along with the experimental data (for smooth walls). The mass flow and the axial thrust coefficients progressively decrease from smooth to rough wall. However, the effect of roughness is more pronounced for the nozzle with area ratio 1.09 (nozzle A1) than with the area ratio 8.81 (nozzle B1). C_d is changed very little by the roughness effects for both nozzle configurations. The axial thrust coefficient, on the other hand, decreases (progressively) with increases in roughness height, more so in the case of nozzle A1 than nozzle B1.

To analyze the effect of wall roughness on the thickness of the viscous layer (at the wall) and on the shear stress at the wall, a viscous reference length is defined as the distance at which the magnitude of k is less than 0.05 times the value in the cell immediately adjacent to the solid wall. The nondimensional distance $y^+_{\rm ref}$ at this reference point is determined. Figures 7 and 8 show the variation of this $y^+_{\rm ref}$ and the distribution of wall shear stress $\tau_{\rm wall}$ for the two nozzles A1 and B1. It is evident from Figs. 7 and 8 that the $y^+_{\rm ref}$ value is substantially increased for the flow with rough wall and they also indicate an increase in the $y^+_{\rm ref}$ with an increase in roughness height. The location of peak values of $y^+_{\rm ref}$ correspond to the locations where the compression wave is incident on the wall, thereby causing a thickening of the viscous layer. The thicker viscous layer results in a reduction of the area available for the core flow and a streamwise shift in the location of the peaks in $y^+_{\rm ref}$. The reduction in the area available for the core flow results in a reduction in the strength of the compression leading to a smaller shock-induced total pressure loss. The variation of $\tau_{\rm wall}$ shows a similar trend, as observed in the case of $y^+_{\rm ref}$. Again, the impact of increase in roughness height is seen to be more pronounced in the case of nozzle A1 than nozzle B1.

The impact of viscous/roughness effects on the overall losses can be analyzed by considering the loss associated with skin-friction. To consider the impact of roughness height on viscous losses, an average skin-friction coefficient is defined (see Appendix for definition). Because the two curves were essentially parallel to one another, the losses associated with skin-friction effects are quite similar for both nozzles. The magnitude of the average skin-friction coefficient was larger

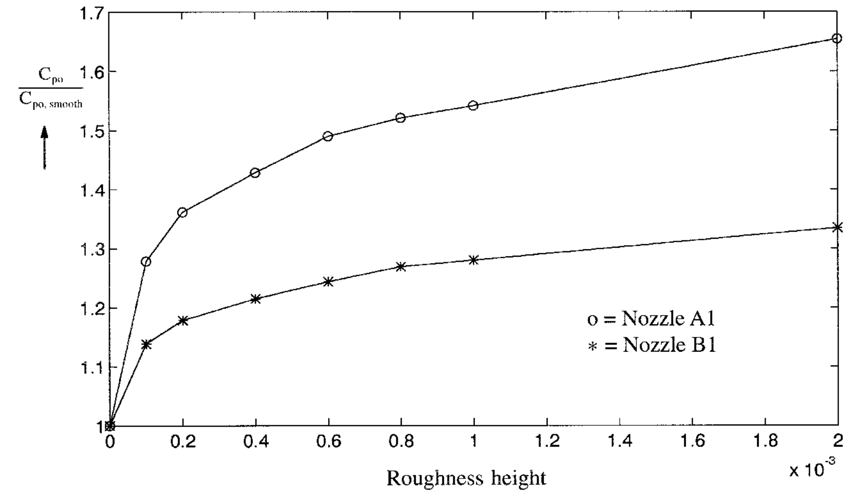

Fig. 10 Computed variation of normalized, total pressure loss coefficient with k_r.

for the case of flow through nozzle A1 than that for nozzle B1. The ratio $\bar{C}_f/\bar{C}_{f\,\mathrm{smooth}}$ is plotted in Fig. 9, as a function of the roughness height. The variation in the skin-friction coefficient (as a function of roughness height) for the two nozzles is reminiscent of the flow over flat-plate boundary layers,[5] in the sense that the variation of skin-friction seems to be independent of the Mach number variations in the core flow. While this could be considered to be an artifact of the wall-function treatment, the fact that the data points for two different nozzle flowfields seem to collapse onto a single curve is too much of a coincidence to ignore. It can be seen from this plot that the losses associated with skin-friction are essentially independent of the nozzle area ratio (thereby the Mach number variation) and are a function of the roughness height only. A simple least-squares fit was used to obtain a third-order polynomial expression relating the variation in skin-friction as a function of the roughness height. This curve fit is shown as the solid line in Fig. 9. The third-order polynomial is given as

$$\mathcal{F}(k_r) = a \times k_r^3 + b \times k_r^2 + c \times k_r + d \tag{26}$$

where $a = 2.6304 \times 10^8$; $b = -1.014 \times 10^6$; $c = 1.465 \times 10^3$, and $d = 1.309$.

Another parameter that can be used to gauge the performance of a nozzle is the total pressure loss coefficient C_{p0}, which is defined in the Appendix. The coefficient C_{p0} is useful in examining the loss in total pressure associated with the flow through the nozzle configuration. The values of the coefficient C_{p0} for the two nozzle configurations is tabulated in Table 4. The variation of the ratio $C_{p0}/C_{p0,\,\mathrm{smooth}}$ is plotted in Fig. 10. It is evident from the values listed in Table 4 and from the plots shown in Fig. 10 that while the magnitude of the loss is larger for the flow through nozzle B1, the effect of roughness is seen to be more pronounced in the flow through nozzle A1. The total axial thrust F_a and the total viscous force F_w are defined in the following equations:

$$F_a = \text{total axial thrust} = \int_{\mathrm{exit}} \rho u^2 \,\mathrm{d}y + \int_{\mathrm{exit}} (p - p_{\mathrm{amb}}) \,\mathrm{d}y \tag{27}$$

$$F_w = \text{total viscous force} = 2.0 \left(\int_{\mathrm{wall}} \tau_{\mathrm{wall}} \,\mathrm{d}s \right) \tag{28}$$

where ds is distance along the wall.

The change in axial thrust and the viscous force is computed relative to the baseline case, i.e., the turbulent flow over smooth walls.

$$\Delta F_a = F_a\big|_{\mathrm{rough}} - F_a\big|_{\mathrm{smooth}} \tag{29}$$

$$\Delta F_w = F_w\big|_{\mathrm{rough}} - F_w\big|_{\mathrm{smooth}} \tag{30}$$

The values are tabulated in Table 5, and Fig. 11 shows a plot of the loss in axial thrust and the change in viscous drag caused by shear stress at the wall, as a function of the roughness height.

Table 5 Nondimensional total thrust and viscous drag

Case	F_a	F_w
a) Nozzle A1		
Smooth: Turbulent	0.3651	0.00350
Rough wall: $k_r = 0.0001$	0.3639	0.0051
Rough wall: $k_r = 0.0002$	0.3634	0.0056
Rough wall: $k_r = 0.0004$	0.3630	0.00617
Rough wall: $k_r = 0.0006$	0.3627	0.00654
Rough wall: $k_r = 0.0008$	0.3622	0.00681
Rough wall: $k_r = 0.001$	0.3620	0.00703
Rough wall: $k_r = 0.002$	0.3615	0.00780
b) Nozzle B1		
Smooth: Turbulent	0.4803	0.00309
Rough wall: $k_r = 0.0001$	0.4795	0.00435
Rough wall: $k_r = 0.0002$	0.4793	0.00481
Rough wall: $k_r = 0.0004$	0.4790	0.00539
Rough wall: $k_r = 0.0006$	0.4788	0.00578
Rough wall: $k_r = 0.0008$	0.4786	0.00608
Rough wall: $k_r = 0.001$	0.4786	0.00634
Rough wall: $k_r = 0.002$	0.4782	0.00724

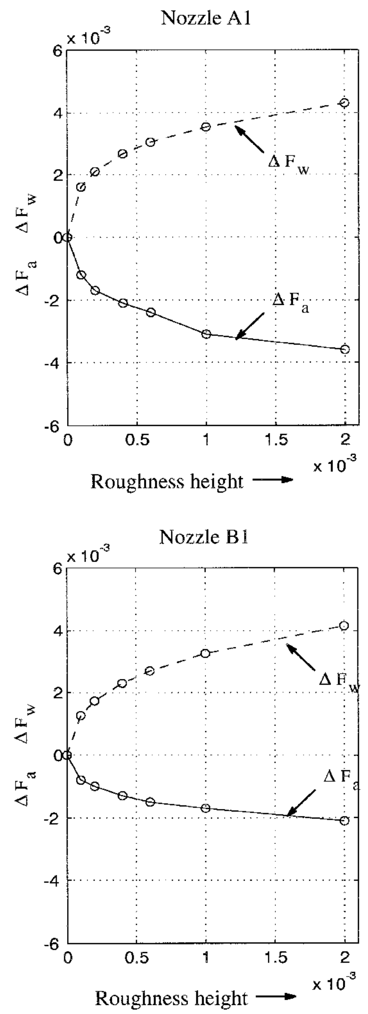

Fig. 11 Computed values of loss in axial thrust F_a and an increase in viscous loss F_w relative to the baseline, i.e., the smooth-wall (turbulent) case.

In Fig. 11, it can be observed that there is an increase in viscous losses (as indicated by an increase in ΔF_w) with an increase in roughness height, and the trend is consistent for both nozzle geometries. Also, there is a decrease in the total axial thrust with an increase in roughness height. In Fig. 11, it can also be seen that the change in ΔF_a is smaller than the rate at which the losses associated with skin-friction/roughness change (as indicated by the change in ΔF_w), implying that there must be a reduction in the other losses (associated with the flowfield). The total loss in the flowfield is a sum of the skin-friction drag and the shock-induced loss. Therefore, in the nozzle flowfield there must be a reduction in the losses associated with the shock system. The overall losses associated with the turbulent flow through the converging–diverging nozzle are seen to be the result of a tradeoff between the reduction in the total pressure loss and an increase in the viscous/roughness-induced losses (indicated by $\bar{C}_f$).

V. Conclusions

The shocks in the flow through the nozzle are smeared by the presence of rough walls while the frictional force on the nozzle wall increases because of the growth of the viscous layer and the enhanced momentum exchange in the wall region. Wall roughness causes increased wall shear stress but reduces the strength of the shocks in the diverging channel. There is a tradeoff between shock-induced losses and viscous/roughness-induced losses. The effect of roughness is more pronounced for the nozzle with the smaller area ratio than for the larger area-ratio nozzle. The effect is true in terms of both the static pressure rise and the decrease in the axial thrust coefficient.

The losses associated with skin-friction indicate that the Mach number variation has very little effect on the predicted values of the ratio ($\bar{C}_f/\bar{C}_{f\,\mathrm{smooth}}$), similar to the observations in the literature for flat-plate boundary layers. A very interesting implication is that for flow in the same regime, one can estimate the effect of the wall roughness on the skin-friction in different flow conditions and geometries based on the analysis of a single set of roughness data.

Appendix: Aerodynamic Coefficients

Mass Flow Coefficient

All of the dependent variables are nondimensionalized by the inlet static pressure, density, speed of sound, and the spatial coordinates by the inlet height. The actual mass flow at the exit of the nozzle is given by

$$\dot{m} = \sum_{\mathrm{exit}} \rho u \Delta A \tag{A1}$$

where ΔA is the incremental area. The ideal mass flow is given as

$$\dot{m}_i = \frac{A p_0}{\sqrt{R T_0}} \sqrt{\gamma \left(\frac{2}{\gamma + 1}\right)^{(\gamma+1)/(\gamma-1)}} \tag{A2}$$

The coefficient C_d

$$C_d = \dot{m}/\dot{m}_i \tag{A3}$$

Axial Thrust Coefficient

Actual thrust vector

$$\boldsymbol{F} = \sum_{\mathrm{exit}} \dot{m}\boldsymbol{v} + \sum_{\mathrm{exit}} (p_s - p_{\mathrm{amb}})\, \mathrm{d}\boldsymbol{A} \tag{A4}$$

Actual thrust in the axial direction (x component of the thrust vector):

$$F_x = \sum_{\mathrm{exit}} \rho u^2 \Delta y + \sum_{\mathrm{exit}} (p_s - p_{\mathrm{amb}}) \Delta A \tag{A5}$$

The ideal thrust is given by

$$F_i = A_j p_0 \sqrt{\frac{2\gamma^2}{\gamma - 1}\left(\frac{2}{\gamma + 1}\right)^{(\gamma+1)/(\gamma-1)} \left[1 - \left(\frac{p_{\mathrm{amb}}}{p_0}\right)^{(\gamma-1)/\gamma}\right]} \tag{A6}$$

The coefficient C_F

$$C_F = F_x/F_i \tag{A7}$$

Average Skin-Friction Coefficient

Average wall shear stress (along the wall)

$$\tau_{\mathrm{wall}}\big|_{\mathrm{av}} = \int_{\mathrm{inlet}}^{\mathrm{exit}} \tau_{\mathrm{wall}}\, \mathrm{d}s \bigg/ \int_{\mathrm{inlet}}^{\mathrm{exit}} \mathrm{d}s \tag{A8}$$

where the shear stress is nondimensionalized by the inlet pressure.

Average skin-friction coefficient

$$\bar{C}_f = \frac{\tau_{\mathrm{wall}}\big|_{\mathrm{av}}}{\frac{1}{2}\rho U_{\mathrm{inlet}}^2} \tag{A9}$$

Total Pressure Loss Coefficient

Total pressure at the inlet

$$P_{0i} = \int_{\text{inlet}} [(p_0) \times \rho U] \, dy \Bigg/ \int_{\text{inlet}} \rho U \, dy \qquad (A10)$$

Total pressure at the exit

$$P_{0e} = \int_{\text{exit}} [(p_0) \times \rho U] \, dy \Bigg/ \int_{\text{exit}} \rho U \, dy \qquad (A11)$$

where p_0 is calculated as

$$p_0 = p \times \{1 + [(\gamma - 1)/2]M^2\}^{\gamma/(\gamma-1)} \qquad (A12)$$

Total pressure loss coefficient

$$C_{p0} = (P_{0i} - P_{0e})/P_{0i} \qquad (A13)$$

Acknowledgement

This work was supported, in part, by the Pratt and Whitney Engine Company.

References

[1]Hill, P. G., and Peterson, C. R., *Mechanics and Thermodynamics of Propulsion*, 2nd ed., Addison–Wesley, Reading, MA, 1992.

[2]Schlichting, H., *Boundary Layer Theory*, 6th ed., 1979, McGraw–Hill, New York, 1979.

[3]Thompson, P. A., *Compressible Fluid Dynamics*, McGraw–Hill, New York, 1972.

[4]Liepmann, H. W., and Goddard, F. E., "Note on the Mach Number Effect Upon the Skin-Friction of Rough Surfaces," *Journal of Aerospace Science*, Vol. 24, 1957, p. 784.

[5]Goddard, F. E., "Effect of Uniformly Distributed Roughness on Skin-Friction Drag at Supersonic Speeds," *Journal of Aerospace Science*, Vol. 26, 1959, pp. 1–15.

[6]Wilcox, D. C., *Turbulence Modeling for CFD*, DCW Industries, Inc., La Canada, CA, 1992.

[7]Cebeci, T., and Chang, K. C., "Calculation of Incompressible Rough-Wall Boundary Layer Flows," *AIAA Journal*, Vol. 16, 1978, pp. 730–735.

[8]Lin, T. C., and Bywater, R. J., "Turbulence Models for High-Speed Rough-Wall Boundary Layers," *AIAA Journal*, Vol. 20, 1982, pp. 325–333.

[9]Christoph, G. H., and Pletcher, R. H., "Prediction of Rough-Wall Skin-Friction and Heat Transfer," *AIAA Journal*, Vol. 21, 1983, pp. 509–515.

[10]Taylor, R. P., Coleman, H. W., and Hodge, B. K., "Prediction of Rough-Wall Skin-Friction Using a Discrete Element Approach," *Journal of Fluids Engineering*, Vol. 107, 1985, pp. 251–257.

[11]Tarada, F., "Prediction of Rough-Wall Boundary Layers Using a Low-Reynolds Number k-ε Model," *International Journal of Heat and Fluid Flow*, Vol. 11, 1990, pp. 331–345.

[12]Rotta, J. C., "Turbulent Boundary Layers in Incompressible Flow," *Progress in Aerospace Sciences*, Vol. 2, 1962, pp. 1–220.

[13]Krogstad, P., "Modification of the Van Driest Damping Function to Include the Effects of Surface Roughness," *AIAA Journal*, Vol. 29, 1991, pp. 888–894.

[14]Krishnamurty, V. S., "Effect of Compressibility on the Turbulence Structure and Its Modelling," Ph.D. Dissertation, Univ. of Florida, Gainesville, FL, 1996.

[15]Shyy, W., Thakur, S. S., Ouyang, H., Liu, J., and Blosch, E. L., *Computational Techniques for Complex Transport Phenomena*, Cambridge Univ. Press, New York, 1997.

[16]White, F. M., *Viscous Fluid Flow*, 2nd ed., McGraw–Hill, New York, 1991.

[17]Koh, Y.-M., "Turbulent Flow near a Rough Wall," *Journal of Fluids Engineering*, Vol. 114, 1992, pp. 537–542.

[18]Mason, M. L., Putnam, L. E., and Re, R. J., "The Effect of Throat Contouring on Two-Dimensional Converging-Diverging Nozzles at Static Conditions," NASA TP 1704, 1980.

[19]Jameson, A., Schmidt, W., and Turkel, E., "Numerical Solutions of the Euler Equations by Finite-Volume Methods with Runge-Kutta Time Stepping Schemes," AIAA Paper 81-1259, 1981.

[20]Shuen, J.-S., "Upwind Differencing and LU Factorization for Chemical Non-Equilibrium Navier-Stokes Equation," *Journal of Computational Physics*, Vol. 99, 1992, pp. 233–250.

[21]Sarkar, S., Erlebacher, G., Hussaini, M. Y., and Kreiss, H. O., "The Analysis and Modelling of Dilatational Terms in Compressible Turbulence," *Journal of Fluid Mechanics*, Vol. 227, 1991, pp. 473–493.